Probing disorder and dynamics in composite electrolytes of an organic ionic plastic crystal and lithium functionalised acrylic polymer nanoparticles

Yady García [a],[*], Luca Porcarelli [a],[b], Haijin Zhu [a], Maria Forsyth [a],[b],[c], David Mecerreyes [b],[c], Luke A. O'Dell [a]

[a] Institute for Frontier Materials and the ARC Centre of Excellence for Electromaterials Science, Deakin University, Geelong, VIC 3216, Australia
[b] POLYMAT University of the Basque Country UPV/EHU, Joxe Mari Korta Center, Donostia–San Sebastian 20018, Spain
[c] Ikerbasque, Basque Foundation for Science, Bilbao, Spain

ARTICLE INFO

ABSTRACT

Solid composite electrolytes combining an ionic molecular phase to facilitate ion transport with a polymeric component to provide mechanical strength are promising material for solid-state batteries. However, the structure-property relationships of these complex composites are not fully understood. Herein we study composites combining the non-flammability and thermal stability of the organic ionic plastic crystal (OIPC) N-methyl-N-ethylpyrrolidinium bis(trifluoromethanesulfonyl) amide [C$_2$mpyr][TFSI] with the mechanical strength of acrylic polymer nanoparticles functionalised with sulphonamide groups having lithium counter-cations. The effect of the formation of interfaces and interfacial regions between the OIPC and polymer nanoparticle on the thermal stability, ion transport, morphology and ion dynamics were studied. It was found that the composites where an interphase was formed by local mixing of the polymer with the OIPC upon heating showed higher local disorder in the OIPC phase and enhanced ion transport in comparison with the as-prepared composites. In addition, doping the composite with LiTFSI salt led to further structural disorder in the OIPC and a selective increase in lithium-ion mobility. Such an improved fundamental understanding of structure, dynamics and interfacial regions in solid electrolyte composites can inform the design of OIPC-polymer nanoparticle composites with enhanced properties for application as solid electrolyte in batteries.

1. Introduction

The components of energy-storage devices, such as the electrolyte and electrodes, interact via interfaces and interphases, which play a key role in regulating the transport of matter and charge, and can determine the extrinsic activity, stability and functionality of a device [1,2]. For example, composite electrodes may contain an active material, polymeric binders that provide mechanical stability and conductive diluents such as carbon black, to facilitate charge transport to the active material [3], while the formation of the solid electrolyte interphase (SEI) layer plays a key role in passivating the electrode surface. Where possible, it is desirable to design interfaces and interphases with specific properties such as enhanced ion transport that can contribute to the improved functionality and reliability of the device [4]. Here we define an interface to be the point at which two different components meet, and an interphase to be a region distinct from the pure components themselves (e.g. a region with enhanced structural disorder or dynamics, or where

the components have mixed together). Important advances towards safer operational devices have been achieved through solid-state electrolytes. Their inherent mechanisms, such as their low diffusion of matter, allow for control over the interphase growth and for stabilization of the electrodes (e.g. Li metal) [1,5]. Solid-state electrolytes can be inorganic (perovskite, garnet, sulphide-type materials, etc.) or organic (ionic plastic crystals (OIPCs), polymers and composite systems) and typically exhibit ionic conductivities up to around the order of 10^{-3} S cm^{-1} at room temperature [6].

Composite solid electrolytes are a very promising approach as they can combine the advantageous properties of their components [7,8]. For example, composites between OIPCs and polymer nanoparticles have recently been developed that combine the ionic conductivity, non-flammability, non-volatility, plasticity, electrochemical, and thermal stability of OIPCs, while at the same time offering the mechanical stability (and potentially also chemical functionality) provided by the polymer [9,10]. In these electrolyte materials the formation of interfaces

and interphases has a critical function in achieving the desired properties. A structural model to describe the kind of interphases and interfacial regions present in these composites has been proposed by Nti and collaborators. This was based on the disruption of the ordered (N-ethyl N-methyl pyrrolidinium bis(fluorosulfonyl)imide ([C₂mpyr][FSI]) OIPC phase after the addition of two different polymer nanoparticles (polyvinylidene fluoride (PVDF) and polystyrene (PS)) and an analysis of the interaction/affinity between those components [11].

However, the ionic transport mechanisms in OIPC-polymer composites are still a matter of study and it has been proposed that the increase in ionic conductivity observed in such composites (relative to the pure OIPC) is associated with the formation of an interphase between the OIPCs and polymer nanoparticles [11]. This interphase may feature both increased structural disorder and dynamics, resulting in an enhancement in local ion transport. It has been proposed that the higher bulk ionic conductivity is attained when this interphase forms a continuous network through the materials, termed the percolation threshold [8]. This highlights the significance of understanding the effects of interphase phenomena that take place in these materials.

The experimental characterization of composite interfaces and interphases can be challenging due to their dimensions, complexity, morphology and inherent disorder, and this increases the difficulty of understanding their formation and properties in terms of the interfacial structures and chemistries [12,13]. Many techniques such as X-ray diffraction, electron microscopy, and various forms of spectroscopy have been used to understand interfaces. Solid-state nuclear magnetic resonance (SSNMR) is a powerful technique for studying local disorder and dynamics in hard or soft solids, amorphous, inhomogeneous or crystalline materials that can co-exist in energy storage materials [14]. In solid OIPCs, polymers and composites electrolytes, ^{7}Li, ^{19}F, and ^{1}H NMR have been implemented to study the ion dynamics via line width analysis. NMR signals from solid powder samples are generally broadened by interactions determined by the rigid-lattice at low temperatures. As the ion jump rates approach or exceed the NMR interaction frequencies at high temperatures, peak narrowing is observed. Thus, two components can often be distinguished, a narrow peak representing a mobile ion fraction in a disordered/dynamic region such as an interphase or a grain boundary, and a broad peak representing the less mobile ion fraction in a more ordered region in the material [15]. In previous studies of [C₂mpyr][TFSI] and PVDF nanoparticle composites it was suggested that the formation of disordered interphases led to an enhancement in ionic conductivity of around one order of magnitude in the composite with 10 v% of PVDF nanoparticles at 30 °C and this further increased with increasing v% of the polymer [16]. This was also confirmed by the narrow peaks observed in the ^{1}H and ^{19}F NMR spectra after the addition of PVDF to the composite and suggested that a fraction of ions becomes highly mobile.

Ion motions also influence NMR relaxation processes such as longitudinal relaxation (quantified by T_1), offering an additional way to probe their dynamics. For example, ^{7}Li T_1 values at high magnetic field strengths are sensitive to motions on a timescale of ns, corresponding to vibrational motions of the Li ions and their surrounding environment [17]. In the systems studied by Meabe and co-workers, where different concentrations of LiTFSI salt were added to a polymer, the highest conductivity of 3.2×10^{-5} Scm^{-1} at room temperature was observed after adding 30 wt% of LiTFSI. In addition, variable temperature T_1 measurements enabled the calculation of the activation energies, correlation times and quadrupolar constants of the systems. The analysis of these parameters allowed the authors to conclude that as the LiTFSI content was increased, the Li environment became slightly more symmetric due to Li ions coordinated by the TFSI anions rather than the ether oxygens of the polymer. This trend increases with the Li salt content and decreases the lithium ionic conductivity [18].

The Li doping of the OIPC component in polymer-based composites also has been studied. Wang et al. prepared composites by coating a Li doped [C₂mpyr][FSI] layer on commercial PVDF nanoparticles [19].

They observed increasing ion conductivity with mass loading content until 30 wt% of polymer, after which it started to decrease. The conductivity was attributed mainly to the conductive layer coated on the polymer. They also studied the composite after melting the OIPC component and observed a decrease in the ionic conductivity. These results were supported by ^{7}Li NMR linewidth analysis, it was concluded that an interaction between the Li ions and the polymer slow down the Li ion dynamics. Crystalline, Li-rich phases in Li-doped OIPCs can also decrease the ion conductivity. A recent study performed by Nti and collaborators studied the interactions between the OIPC triethyl (methyl)phosphonium tetrafluoroborate [P₁₂₂₂][BF₄] and PVDF nanoparticles as well as the doping of the OIPC. They observed the formation of Li-rich phases in the OIPC lattice after the Li-doping of the OIPC. This phase was associated with poor ion transport properties, but could be suppressed by the addition of PVDF nanoparticles, with the PVDF−OIPC interphase formed in the polymer-based composite increasing the local disorder of the OIPC and leading to enhanced ionic conductivity [20].

The works discussed above demonstrate the extensive efforts that have been made to understand the interfacial properties that enhance or decrease the desired properties of solid electrolytes in composites. Herein, we correlate macroscopic properties such as ion conductivity with the interfacial phenomena in a new chemical architecture of composites consisting of the OIPC [C₂mpyr][TFSI] and lithium functionalised acrylic polymer nanoparticles (see Fig. 1). The polymer nanoparticles consist of a crosslinked methacrylic polymer chain including a side chain featuring a functional co-monomer lithium 1–(3–(methacryloyloxy)propylsulfonyl)–1–(trifluoromethylsulfonyl)imide (LiMTFSI), structurally analogous to the TFSI anion and with lithium ions as the cation [21,22]. These polymer nanoparticles exhibit a glass transition temperature of 122 °C, an average particle size of 95 nm and it was estimated that 80 mol% of the LiMTFSI monomer resides at the surface of the nanoparticles. These composites were designed to take advantage of the intrinsic properties of the OIPC like plasticity, with the mechanical strength and Li ions containing ionic functionalisation of the polymer, and it is anticipated that the formation of interfaces and interphases between these components will promote the ion transport of the Li cations. Additionally, the effect of doping one of the composites with LiTFSI was studied. It was already observed that the addition of Li salt to the pure OIPC increases the ionic conductivity by three orders of magnitude [9] and in these composites it may also promote the compatibility between the polymer and the OIPC.

2. Experimental section

2.1. Preparation of polymer particles: [C₂mpyr][TFSI] composites and LiTFSI: [C₂mpyr][TFSI]: polymer nanoparticle composite

The [C₂mpyr][TFSI] OIPC and polymer nanoparticles were synthesized following previously established procedures [9,21]. Lithium bis(trifluoromethanesulfonyl) imide LiTFSI was purchased from Solvay and used as received. The densities of [C₂mpyr][TFSI] and the polymer nanoparticles were measured at 25 °C using a helium pycnometer and correspond to 1.43 g/cm^3 and 1.85 g/cm^3, respectively. Four polymer-based composites containing different volume percentages of polymer nanoparticles (10, 15, 25 and 30 ($\pm$ 2) v%) were prepared by dissolving calculated amounts of [C₂mpyr][TFSI] and polymer nanoparticles in dry methanol. For the preparation of LiTFSI₀.₁ [C₂mpyr]₀.₉[TFSI]:polymer nanoparticle composite electrolyte, LiTFSI salt and [C₂mpyr][TFSI], in [1:9] molar ratio, were also dissolved in a mix of dry methanol and acetone, LiTFSI and [C₂mpyr][TFSI] represent 12 and 63 ($\pm$ 2) v% of the composite, respectively. Then, 25 ($\pm$ 2) v% of polymer nanoparticles were added into the solution.

The resulting solutions were sonicated and stirred to form uniform suspensions. The suspensions were cast on Petri dishes, and the methanol was quickly evaporated under argon flow at room temperature. The
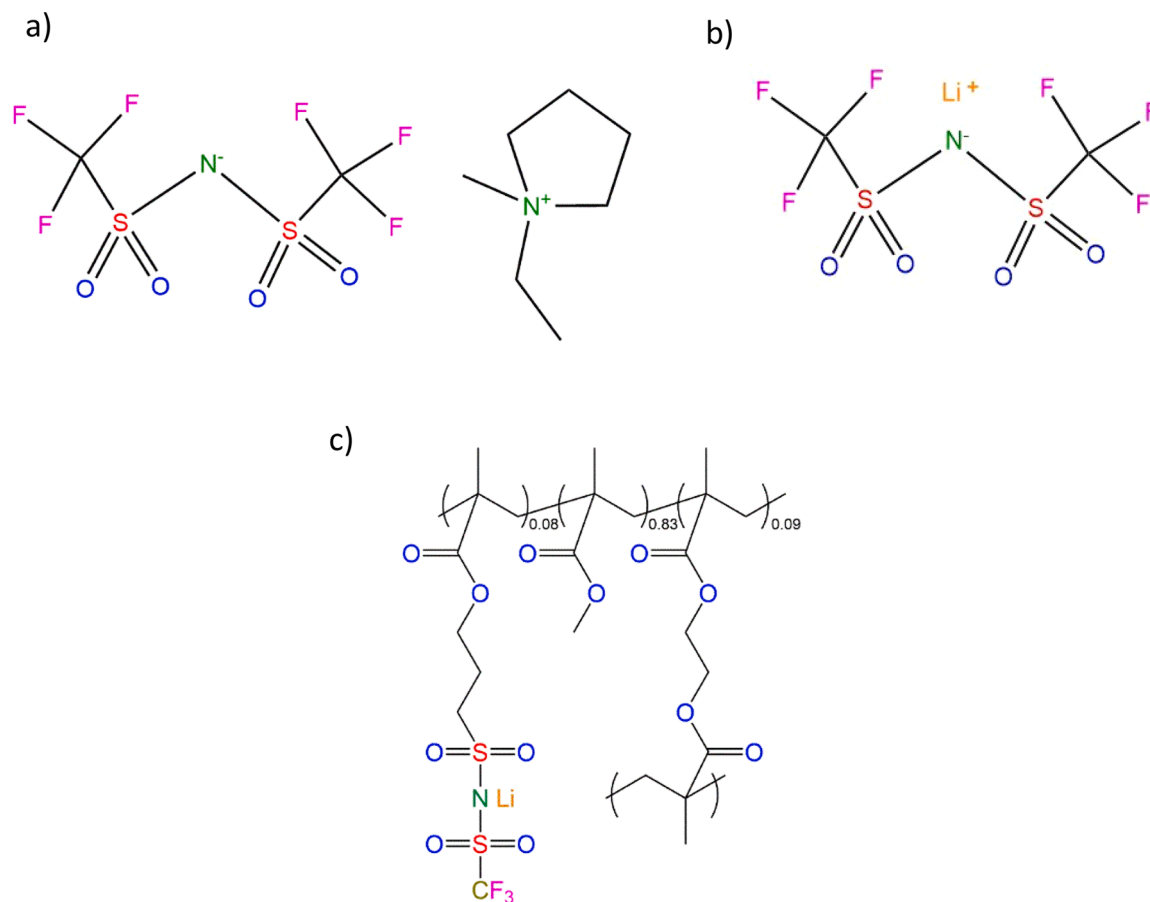
Fig. 1. Molecular structures of (a) the OIPC, (N-methyl N-ethyl pyrrolidinium bis(trifluoromethanesulfonyl)imide [C$_2$mpyr][TFSI], (b) the Li salt, Lithium bis (trifluoromethanesulfonyl) imide and (c) the polymer.

samples were then packed into glass vials and the residual solvent was removed on a Schlenk line at 50 °C for 24 h. A portion of the composites with 25 v% of polymer nanoparticles and doped with LiTFSI were also heated on a Schlenk at 90 °C while stirring for 2 h. The as-prepared 25:75 v% polymer nanoparticles: OIPC and doped composites (unheated) are named as-prepared and as-prepared_doped, respectively, while the samples heated at 90 °C (i.e., melting the OIPC component) are named melted and melted_doped, respectively, throughout the discussion. Finally, all samples were transferred into an argon-filled glove box for storage and preparation for characterization.

2.2. Characterisation

2.2.1. Differential scanning calorimetry (DSC)

DSC measurements of the composites were carried out using a Mettler Toledo DSC1 instrument equipped with STARTeV6.10 software. Approximately 7–12 mg of the composites were packed in aluminium pans in an inert atmosphere and tested over a temperature range of −120 to 140 °C at a scanning rate of 10 °C/min. To investigate the influence of thermal history of the samples, three thermal cycles were performed for each sample. All samples were held at an isothermal temperature of −120 °C for 30 min before heating.

2.2.2. Polarised optical microscopy

The OIPC and composite samples were first prepared for optical microscopy by solvent casting the material directly onto a microscope slide, using the solvents mentioned in Section 2.1, to study the composites as prepared, and secondly by placing the samples on a microscope slide, and squeezed with a glass cover after heating the materials above the melting point of the OIPC in a hot stage. The temperature was

kept at 95 °C for 10 min before a cooling rate of 10 °C/min was used to promote recrystallization. The polymer nanoparticles were placed on a microscope slide as prepared. The images were captured with a polarised optical microscope Nikon Eclipse Ti–U with 100x magnification at room temperature.

2.2.3. Electrochemical impedance spectroscopy (EIS)

The average ionic conductivities of the composites were measured using a biologic MTZ-35 driven by MT-lab software. The dried powder samples were pressed between two stainless steel discs in a sealed KBr die using a hydraulic press under 3 tons of pressure for 5 min. Each pellet of 3 mm thickness was inserted into a hermetically sealed barrel cell. A frequency range of 10 MHz to 1 Hz was studied using a voltage amplitude of 0.01 V with temperature ranging from 30 to 70 °C at 10 °C steps. Data was acquired during three cycles, a heating scan from 30 to 70 °C, a subsequent cooling scan (70 to 30 °C) and finally, another heating scan, with the objective to observe the reproducibility and any hysteresis that might be present. Conductivity values were calculated from Nyquist plots in which the touchdown point of the semi-circle corresponds to the bulk resistance of the ionic conducting media. The Nyquist plots of the composite as prepared and after melting the OIPC component at 30 °C and 50 °C are presented in the supporting information (Fig. S1).

2.2.4. Solid-state MAS NMR (SSNMR)

The study of the molecular-level structure of the pure materials and selected composites by solid-state MAS NMR experiments was carried out with a Bruker Avance III 300 MHz wide-bore spectrometer with a 4 mm H/F-X double resonance MAS probe, at 12 kHz spinning frequency, and Larmor frequencies of 300.13, 75.468, 116.6 MHz for ^{1}H, ^{13}C and ^{7}Li, respectively. Samples were packed and sealed in 4 mm NMR MAS

rotors in an argon-filled glovebox. ^{19}F and ^{7}Li MAS NMR were performed to average the chemical shift anisotropy (CSA) effects by spinning the samples at 54.74° with respect to the external field. A cross polarization (CP) pulse sequence was performed with decoupling to increase the sensitivity of ^{13}C by transferring magnetization from abundant nuclei like ^{1}H and ^{19}F. Then, ^{1}H–^{13}C CPMAS (with ^{1}H decoupling) spectra of the neat OIPC, polymer nanoparticles and selected composites were acquired. Solid sodium fluoride (NaF), lithium chloride (LiCl) and water were used as chemical shift references for ^{19}F (−224.2 ppm), ^{7}Li (0.0 ppm) and ^{1}H (4.8 ppm), respectively.

Static (i.e., without MAS) SSNMR experiments to study dynamics in the pure materials and selected composites were carried out with a Bruker Avance III 500 MHz wide-bore spectrometer with Larmor frequencies of 194.3 and 470.4 MHz, for ^{7}Li and ^{19}F, and using a 5 mm HX static probe. Spectra were acquired with a single pulse experiment using a 90° pulse in the case of ^{1}H and ^{7}Li and Hahn echo experiments for ^{19}F with an echo time of 5 μs. The sample temperatures were calibrated using the ^{207}Pb signal from lead nitrate [23]. Line widths reported herein, correspond to the full width at half of maximum intensity (FWHM) of the spectral peak measured as a function of temperature. The sample temperature was equilibrated at each temperature for 10 min. The temperature variation of the ^{7}Li and ^{19}F spin lattice relaxation times (T_1) were also measured over the same temperature range using a

saturation recovery pulse sequence. Sixteen relaxation delays were used, varying from 0.1 ms to 60 s depending on the T_1 value. The resulting data were fitted using a single exponential function using the Bruker TopSpin software.

The ^{19}F CSA patterns of the pure OIPC were also studied using static Hahn echo experiments at −20 °C and 20 °C and echo delays from 5 μs to 0.5 s. These measurements were performed in a Bruker Avance III 500 MHz wide-bore spectrometer with a 4 mm H/F-X-Y triple resonance MAS probe equipped which enabled the use of ^{1}H decoupling to remove the ^{1}H-^{19}F dipolar couplings.

3. Results and discussion

3.1. Thermal analysis

3.1.1. Polymer nanoparticles: [C₂mpyr][TFSI] composites

The DSC thermal traces of pure [C₂mpyr][TFSI] and the polymer nanoparticles: [C₂mpyr][TFSI] composites containing 10, 15, 25 and 30 v% of polymer nanoparticles are presented in Fig. 2. During the first heating cycle, the pure OIPC goes through three solid–solid endothermic phase transitions noted as IV → III, III → II, and II → I with onset temperatures at approximately −85, 16 and 45 °C, respectively, before melting at 91 °C, as reported previously [9]. These phase transitions are
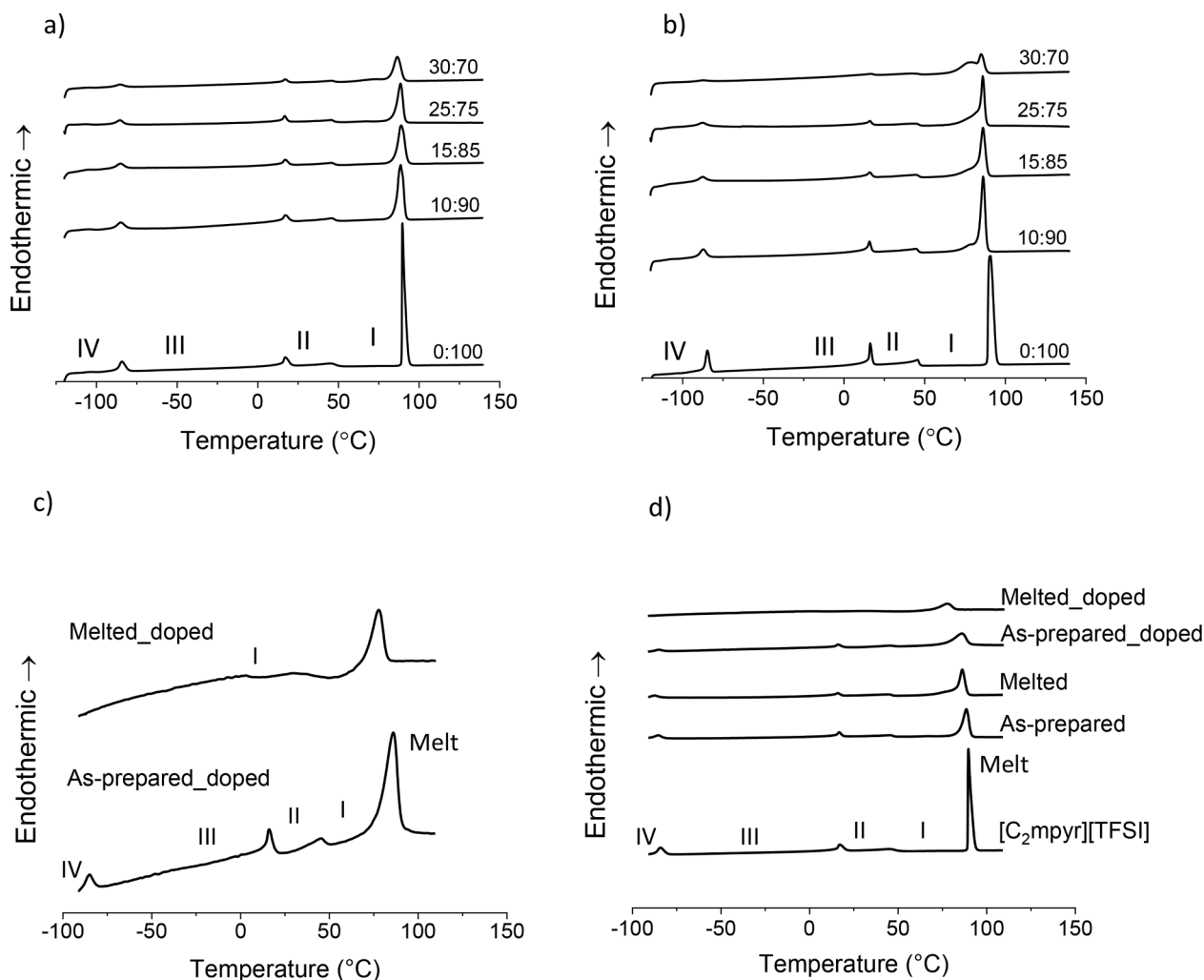

Fig. 2. DSC of (a) first and (b) second heating traces of the neat [C₂mpyr][TFSI] and the polymer nanoparticles: [C₂mpyr][TFSI] composites as a function of the concentration of polymer particle (10, 15, 25 and 30 v%), (c) first and second heating traces of Li doped 25 v% polymer nanoparticles: [C₂mpyr][TFSI] composite noted as-prepared_doped and melted_doped, respectively and (d) comparison between the neat OIPC, 25 v% polymer nanoparticles: [C₂mpyr][TFSI] composites (as-prepared and melted) and Li doped 25 v% polymer nanoparticles: [C₂mpyr][TFSI] composite (as-prepared_doped and melted_doped).

also observed in the composites but with a lower enthalpy (see Table S1 a). Moreover, the melting peak in the composites is broader and its onset temperature is shifted from 91 to 88 °C. In the second heating cycle of the neat OIPC, the peaks of the phase transitions get narrower while the melting peak gets broader which suggests that the crystallinity of the OIPC component of these composites increased after melting and subsequent cooling (see Fig. 2b).

In the DSC traces of the composites, the phase transitions of the OIPC component can still be observed during the second heating cycle but with a lower intensity compared to the first heating and shifted to slightly lower temperatures (see Fig. 2a and b). These peaks also become broader as the concentration of polymer nanoparticles increases, reflecting an increasing level of disorder in the OIPC component.

In addition, in the second heating trace of the composites (without additional Li salt) the appearance of a new peak with an onset temperature at 60 °C can be observed to the left of the melting peak. This new peak, which is not observed in the first heating trace, becomes more prominent with the increase in polymer nanoparticle content. The first heating traces of the composites are different to the second due to the melting of the OIPC component between each scan, which enables rearrangement of the OIPC molecules and recrystallization to take place. Prior to this, the interaction of the OIPC and the polymer nanoparticles creates a local disorder in the OIPC, close to the polymer nanoparticles, as can be inferred from the broader melting peaks in Fig. 2a. This local disorder close to the polymer nanoparticles is illustrated schematically in Fig. 3a. The additional melting peak in the DSC (second heating) scans of the composites suggests an additional component, formed after the melting of the OIPC phase, with further increased disorder (relative to the pure OIPC) resulting in a local decrease in the OIPC melting temperature [11,24]. This peak indicates the formation of an interphase where the OIPC interacts with (and possibly mixes with) the polymer

chains during the melting of the OIPC component (Fig. 3b). This region may also promote further disorder in the local OIPC structure as proposed by Nti and co-workers [11]. The fact that the interphase melting peak overlaps with the melting peak of the pure OIPC component in the second heating trace of the composites hinders the calculation and comparison of the entropy and enthalpy for these two components (peak deconvolution is extremely difficult due to the asymmetric shape of these peaks). These observations are also supported by a suppressing effect in the enthalpy of the OIPC in the second heating in comparison with the first heating and indicate that the composite systems become more disordered (see Table S1 a).

3.1.2. Li salt – polymer nanoparticle composite

The effects of the addition of 1 mol% LiTFSI salt into the 25 v% polymer nanoparticles: [C$_2$mpyr][TFSI] composite was studied during the first (as-preapred_doped) and second (melted_doped) heating, and the DSC thermal traces for this sample are presented in Fig. 2c. This concentration of Li salt was selected based on the increase of ionic conductivity observed in a previous study of the pure OIPC [9,25].

The solid-solid phase transitions are observed in the composite doped with LiTFSI salt during the first heating (as-preapred_doped), and the addition of LiTFSI salt decreases the enthalpy of the OIPC further suggesting that the local environment of the OIPC become more disordered (see Table S1 b). Furthermore, these transitions are broadened significantly after melting the OIPC component and recording a second heating scan (melted_doped) indicating a high degree of structural disorder within the OIPC; indeed, the near complete absence of the solid-solid phase transitions in the second scan suggests that the OIPC retains its phase I character even at lower temperatures and it is followed by a cold crystallisation before melting.

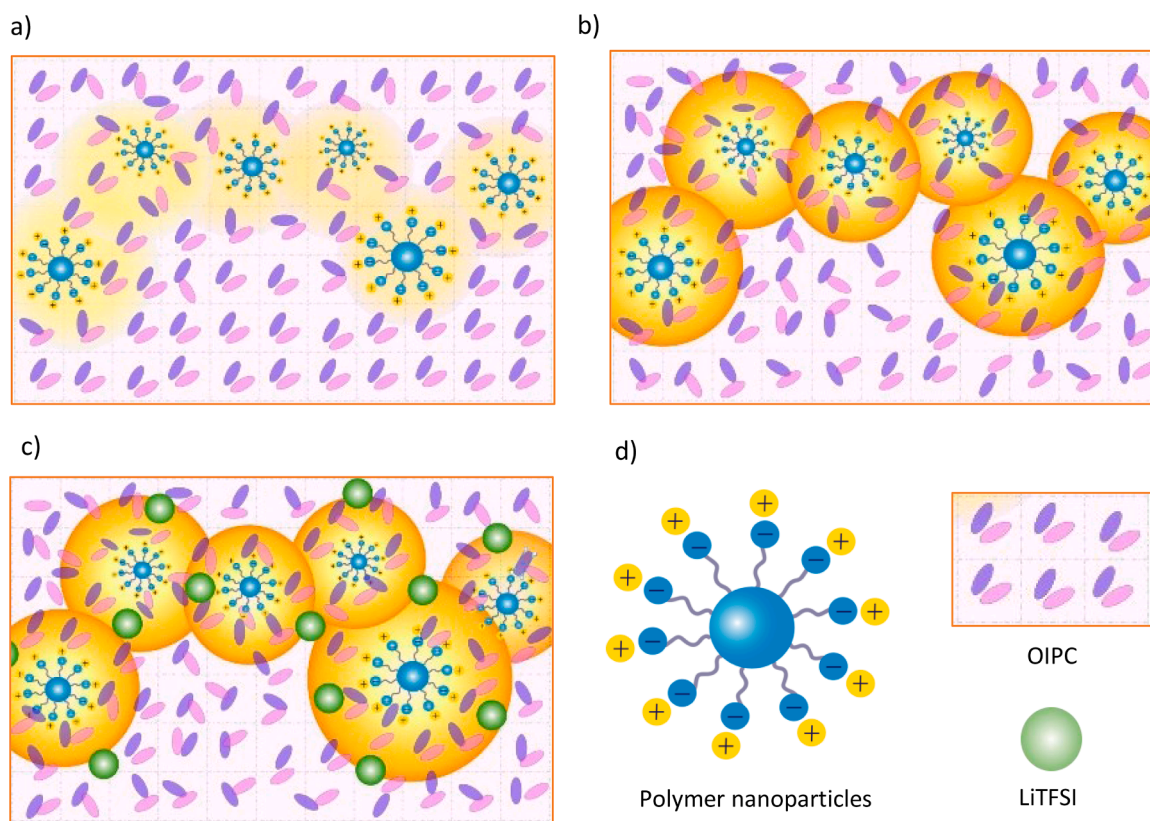The melting peak of the OIPC in the Li-doped composites show onset

Fig. 3. Schematic representations of (a) local disorder in the OIPC component close to the polymer nanoparticles before the melting of the OIPC component, (b) the formation of an interphase (orange region) after further mixing of polymer nanoparticles and the OIPC after melting the OIPC component, with increased disorder in the OIPC component, and (c) doping of the composite with LiTFSI. Schematic representations (d) of the distribution of Li ions in the polymer, the OIPC lattice and LiTFSI.

temperatures shifted to a lower temperature compared with the undoped composites (70 °C during the first heating and at 65 °C during the second heating) as shown in Fig. 2d. In addition, this peak is significantly broadened in the doped system. Thus, more structural disorder seems to be formed in the OIPC component of the composites after adding LiTFSI. It is accepted that in the LiTFSI doped [C₂mpyr][TFSI] a Li rich eutectic solution at grain boundaries of the OIPC is the leading mechanism of conductivity [9]. As a result of the OIPC cations exchanging with Li on the surface of the nanoparticle a further Li doping of the OIPC component occurs. This will also create greater local free volume, disorder, and dynamics.

Thus, we observe the formation of two interfacial regions in the composites before and after doping with Li salt. The first one shows local structural disorder in the OIPC lattice, which is present in the composites as prepared, and will be referred through the document as the "interfacial region". The second one is characterised by further structural disorder in the OIPC lattice because of the deeper mixing of the components of the composites that occurs when the OIPC is melted, and this will be referred to as the "interphase".

3.2. Crystallite morphology

Organic ionic plastic crystals can be optically anisotropic materials and present birefringence as a result of the short-range disorder within their long-range ordered crystalline lattices [26]. On the other hand, completely amorphous materials such as polymers are optically isotropic and do not exhibits birefringence [27]. The morphology of the OIPC and composites was studied qualitatively using an optical microscope to get insights about the crystallite size, structure, and distribution (see Fig. 4). The images were taken at room temperature after solvent casting the samples to study the materials as prepared and after heating the samples above the melting point of the OIPC on a microscope heating stage.

Pure [C₂mpyr][TFSI] in the as prepared state displays a polycrystalline structure of crystal domains larger than 500 μm (Fig. 4a and b). The colors in Fig. 4 represent different orientations of the crystallites delimited by grain boundaries. After adding the polymer nanoparticles some regions with much smaller crystals (< 50 μm) are observed (see Fig. 4c). The image of the as prepared composite with LiTFSI (Fig. 4d)
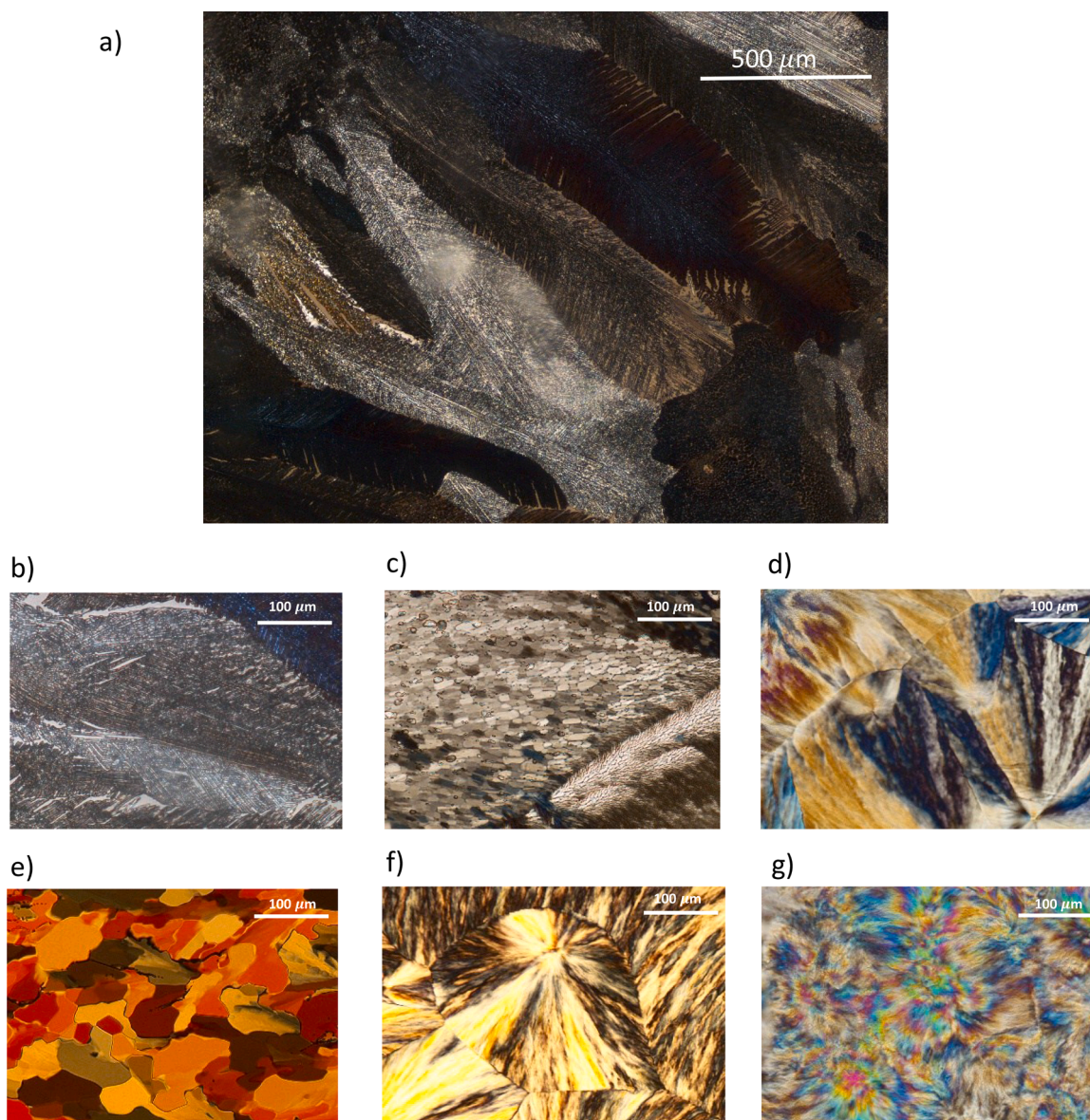

Fig. 4. Polarised optical micrographs of (a) and (b) pure OIPC as prepared, (c) the 25 v% polymer nanoparticles: [C₂mpyr][TFSI] composite as prepared, (d) Li doped composite with LiTFSI as prepared, (e) the OIPC after melting the OIPC component, (f) 25 v% polymer nanoparticles: [C₂mpyr][TFSI] composite after melting the OIPC component, and (g) doped with LiTFSI after melting the OIPC component.

shows more variation in colour indicating different crystal orientations, suggestive of an increased level of disorder in this material than in the as prepared polymer-based composite.

After melting and recrystallisation, the neat OIPC shows smaller crystals on the order of 100 μm with different orientations (see Fig. 4e) indicating that more grain boundaries are formed after melting the OIPC in comparison with the as-prepared sample. After melting the OIPC component in the composite with 25v% of polymer nanoparticles, polycrystalline spherulite-like domains greater than 100 μm in size are observed with a increased amount of grain boundaries than the as-prepared sample (Fig. 4f). This is attributed to the influence of the polymer nanoparticles on the recrystallisation of the OIPC, which may act as nucleation sites and direct the crystal growth. Doping the composite with LiTFSI also leads to the formation of smaller spherulites than those observed after melting the OIPC component in the polymer-based composite thus leading to further reduced domain sizes as seen in Fig. 4g, indicating more structural disorder after doping the composite with Li. These observations again support the increasing disorder observed in the DSC heating traces after melting the OIPC component in the composite with lithium doping.

These images are consistent with the DSC results discussed in the previous section, with smaller crystallites being accompanied by a greater overall level of disordered grain boundary regions. Similar observations have previously been made by Ramos and collaborators in the study of poly(ethylene oxide) (PEO) and OIPCs membrane composites [28], who proposed that the OIPC might be confined by the polymer component during the recrystallisation, further increasing the structural disorder.

3.3. Ionic conductivity measurements

The ionic conductivities of the pure OIPC and a selected composite with 25 v% of polymer nanoparticles as prepared (i.e., as-prepared) and after melting the OIPC component (i.e., melted) and the Li doped composite as prepared (i.e., as-prepared_doped) and after melting the OIPC component (i.e., melted_doped) were measured as a function of temperature through EIS experiments and the results are presented in Fig. 5a. The experiments were performed from 20 to 60 °C to avoid the melting temperature of the OIPC component. The observation of a single well-defined semicircle in the Nyquist plots of all samples (Fig. S1) suggests a single conductivity mechanism is present in all samples.

A general trend of increased conductivity with temperature can be observed for the samples measured. It is also observed that the ionic conductivity for the composite (where the OIPC component is more disordered as observed in the DSC heating traces) is higher than the pure

$[C_2mpyr][TFSI]$ during the first heating (see Fig. 2a). There is no observed jump in conductivity during the transition from phase II to I, implying that this phase transition does not significantly affect the ion conductivity mechanism.

A further increase in ion conductivity in the composite is observed during the second heating (melted, Fig. 5a). This increase in conductivity can be attributed to the formation of the disordered interphase region between the OIPC and polymer components as suggested by DSC results, as well as the larger amount of OIPC grain boundaries observed in the morphology study of the composites (Fig. 4). The interphase and grain boundaries are both expected to feature increased disorder, dynamics, and free volume. Additionally, the $[C_2mpyr]$ cations may undergo exchange with the Li on the polymer nanoparticles surface, there may be a Li doping effect on the OIPC (further discussed through the structural NMR analysis in Section 3.5), that facilitates the ion conductivity.

The as-prepared_doped composite shows similar conductivities at lower temperatures to the pure OIPC suggesting that the interfacial region between the OIPC, polymer nanoparticles and LiTFSI does not improve the average ion mobility until phase I is reached. Conversely, after melting the OIPC component in the doped composite the conductivity is observed to increase significantly (by more than one order of magnitude at 60 °C in comparison with the OIPC). This can be attributed to an increase in the mobility of the ions located in the disordered interphase formed between the OIPC and polymer nanoparticles as a result of the initial exchange between OIPC cations and Li on the polymer nanoparticles that create a partial doping of the OIPC and the further doping of the OIPC after adding LiTFSI leading to a higher conductivity in melted_doped compared to melted (Fig. 5). These observations support the DSC and morphology analysis where more structural disorder is observed in the doped composite after melting the OIPC component in comparison with the as-prepared doped composite. However, the melted_doped showed lower conductivity than the OIPC doped with 0.9 mol% of LiTFSI studied previously [9], which showed conductivity of almost two order of magnitude (i.e., from 10^{-8} to 10^{-6} S cm^{-1}) larger than the OIPC at 27 °C indicating that the polymer nanoparticles restrict the mobility of the ions in the composite in comparison with the doped OIPC.

3.4. Solid-state NMR analysis: structure

The pure $[C_2mpyr][TFSI]$, polymer nanoparticles, and composites with 25:75 v% polymer nanoparticles: $[C_2mpyr][TFSI]$ as prepared (as-prepared) and after melting the OIPC component (melted), as well as the same composite with 1 mol% LiTFSI salt incorporated as prepared (as-
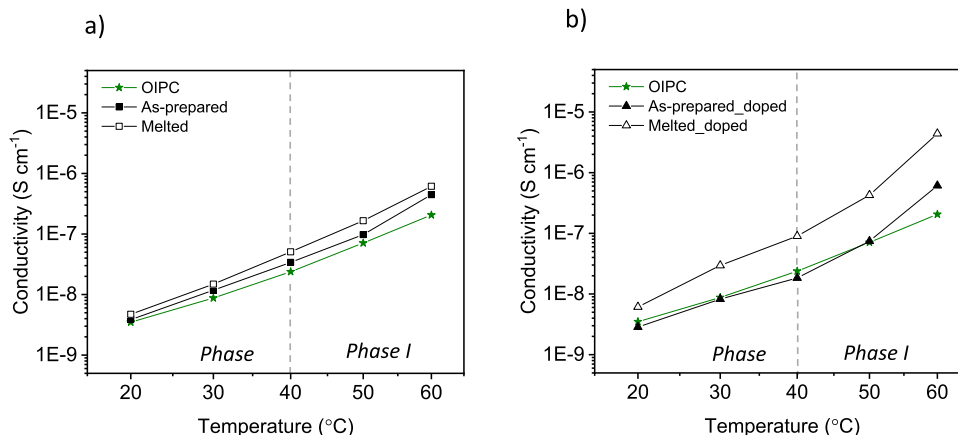

Fig. 5. Ion conductivity as a function of the temperature of (a) the composites with polymer nanoparticles concentration of 25 v% as prepared (as-prepared) and after melting the OIPC component (melted), and (b) the LiTFSI doped composite as prepared (as-prepared_doped) and after melting the OIPC component (melted_doped) against the ion conductivity of $[C_2mpyr][TFSI]$.

prepared_doped) and after melting the OIPC component (melted_doped) were studied by ^{13}C CPMAS and ^{19}F and ^{7}Li MAS NMR experiments. The ^{1}H–^{13}C CPMAS NMR spectra for these samples and the assignment of carbon resonances for the OIPC and the polymer nanoparticles are presented in Fig. 6.

The crystalline structure of the OIPC results in narrower ^{13}C peaks than the signals from the polymer where the carbon sites exist in a locally disordered structure. The as-prepared composite spectrum resembles the pure OIPC, and polymer signals superimposed with slightly broader OIPC peaks shifted to a lower chemical shift, suggesting that the chemical environment of the carbons in the OIPC is altered to some extent by the addition of polymer nanoparticles and that the OIPC and polymer have mixed in the interfacial region. On the other hand, in the melted composite some changes can be observed in the shape and intensity of some of the polymer signals and in the OIPC linewidth of the ^{13}C peaks where the narrower ^{13}C peaks reflects the increase of the local dynamics of the OIPC cations (i.e., rotations) in this composite. In addition, these signals are shifted to a lower chemical shift than in melted composite and suggest that the chemical environment of the OIPC cations was altered after the addition of the polymer nanoparticles, consistent with some mixing with the OIPC component in the melt state.

In the composite doped with the Li salt as prepared, changes in the intensity and broad signals of the carbon environments that come from the polymer are also observed in a similar magnitude to melted_doped composite. The ^{13}C peaks from the OIPC component show similar line-widths than the pure OIPC but are shifted to lower chemical shifts than the as-prepared and melted composites (see Fig. S2), suggesting that the addition of LiTFSI further changes the local environment around the OIPC cations. In addition, a new peak at 180 ppm is observed in both doped composites. This is attributed to an interaction between the Li cation of the Li salt with the electronegative oxygen of the carbonyl groups at the surface of the polymer nanoparticles.

The changes in the chemical environment of the OIPC cation signals indicated by the lower chemical shifts suggest an exchange of these cations with the Li ions on the polymer nanoparticles, as will be discussed later, that allows an initial Li doping of the OIPC in the composites as-prepared and melted and a further doping after adding LiTFSI. These doping effects not only increased local disorder but also local dynamics of the OIPC cations. It should be noted that the ^{13}C signals

from the CF$_3$ groups of the polymer nanoparticles and OIPC are not observed in these spectra due to the use of cross polarisation from ^{1}H.

Changes in the average chemical environment of the Li ions were observed in the composites with respect to the polymer nanoparticles as can be seem in Fig. 7. A broad ^{7}Li MAS NMR peak is observed for the polymer nanoparticles as was expected due to the inherent structural disorder in this material.

In general, the composites showed asymmetric ^{7}Li peak widths with a noticeable shift to lower chemical shifts with respect to the polymer, indicating a change in the surrounding structural environment of the Li ions. In the case of the as-prepared composite, the peak was shifted as a result of the interaction of the Li ions with the surrounding OIPC. Once the OIPC is melted in the composite, the OIPC and polymer components become more intimately mixed and as a result a further shift and broader peak is observed for melted composite, indicative of more structural disorder around the Li ions in the interphase. After doping the composite
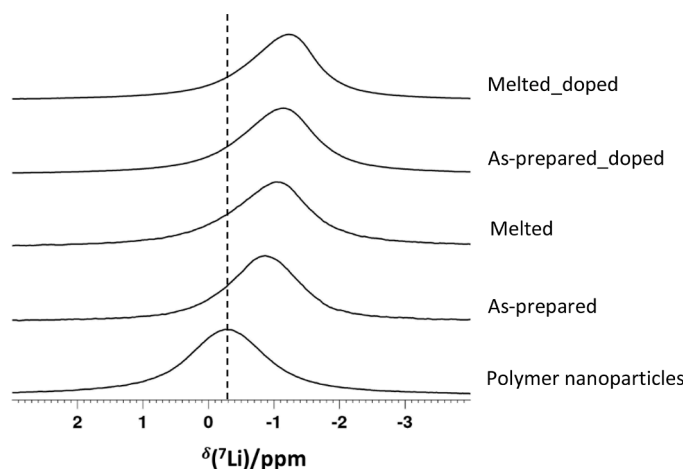

Fig. 7. ^{7}Li MAS NMR spectra of polymer nanoparticles, 25:75 v% polymer nanoparticles: [C$_2$mpyr][TFSI] composites as prepared (as-prepared) and after melting the OIPC component (melted), and Li doped composites as prepared (as-prepared_doped) and after melting the OIPC component (melted_doped).
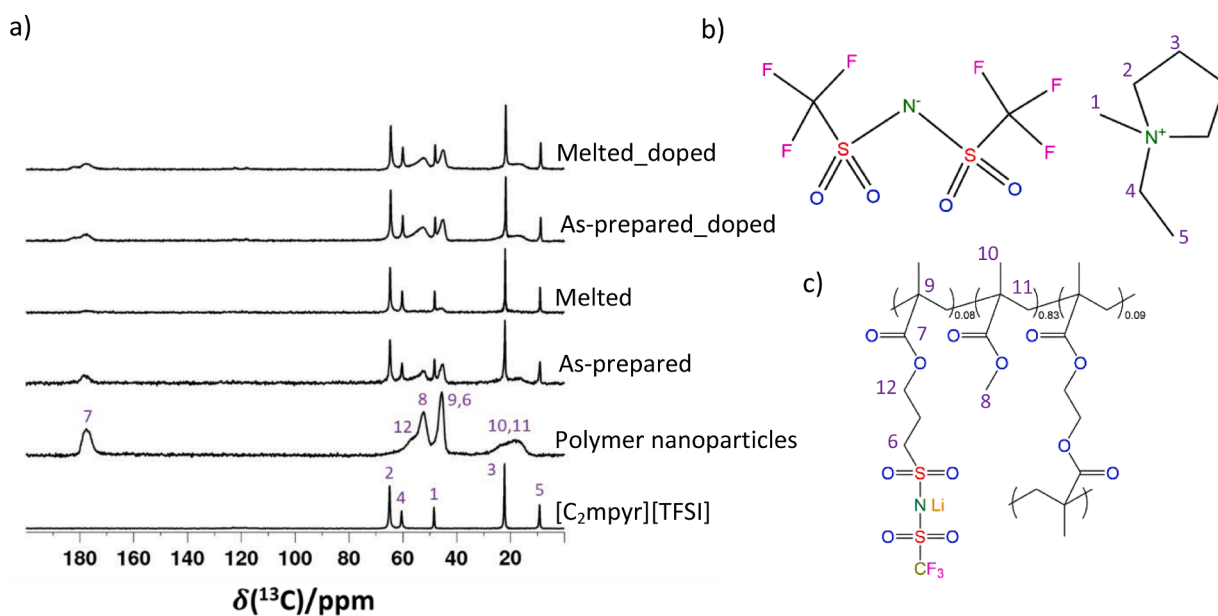

Fig. 6. (a) ^{1}H–^{13}C CPMAS NMR of [C$_2$mpyr][TFSI], polymer, 25:75 v% polymer nanoparticles: [C$_2$mpyr][TFSI] composites as prepared (as-prepared) and after melting the OIPC component (melted), and Li doped composites as prepared (as-prepared_doped) and after melting the OIPC component (melted_doped). Molecular structures of (b) [C$_2$mpyr][TFSI] and c) polymer with partial assignment of the ^{13}C peaks to certain structural sites.

with the Li salt the [7]Li signals in as-prepared_doped and melted_doped appear very slightly further shifted to the right, but are quite similar to the spectrum of melted composite. The changes observed in the shape, linewidth and chemical shift in the composites suggest some type of complexation or exchange of the lithium on the polymer nanoparticles with other anions, in this case with the OIPC cations. This exchange is greater in the composites after melting the OIPC component (i.e., melted and melted_doped) and results in interphases with increased disorder that facilitate the ion conductivity as discussed in Sections 3.1–3.3.

^{19}F MAS NMR spectra were also acquired from the OIPC, polymer nanoparticles and composites, and are shown in Fig. 8. A single ^{19}F isotropic chemical shift is observed for the pure OIPC, polymer nanoparticles and all four composites. However, the ^{19}F signal of the polymer is much broader than that of the OIPC and composites due to the higher level of local structural disorder around the polymer anionic groups.

The ^{19}F spectra of the composites appear very similar to that of the OIPC and this is due to the dominance of the OIPC TFSI signal. However, a slight broadening of the signal observed in the doped composites suggests some increased structural disorder after the addition of LiTFSI. Due to the composition, the broader signal from the anionic polymer groups will show a much lower intensity and is thus somewhat hidden under the sharper TFSI signal (see peak deconvolution in Fig. S3).

Interactions such as chemical shift anisotropy (CSA) are inherent to static ^{19}F NMR spectra and are related to the chemical environment, so can provide information both on the structure (e.g. conformation) and molecular dynamics such as rotations or reorientations of TFSI anions [29]. Therefore, static ^{19}F NMR spectra were also acquired from these samples using a Hahn echo pulse sequence. Additionally, ^{1}H decoupling was used to remove the heteronuclear dipolar interactions with the protons present on the [C₂mpyr] cation, providing sharper ^{19}F CSA patterns. Interestingly, the fitting of the [C₂mpyr][TFSI] static Hahn echo NMR spectrum with a short echo delay time at 20 °C required three distinct CSA patterns (Fig. 9 and Table S2) despite only a single isotropic ^{19}F signal being observed by MAS NMR (Fig. 8).

These CSA patterns are postulated to arise from different conformations of the TFSI anion (i.e., *trans, cis* and *gauche*). Previously, these three different conformations of the TFSI ion were observed in liquid LiTFSI-acetamide electrolytes with molar ratios of 1:2, 1:4, and 1:6 using DFT simulations [30]. It was observed that the *gauche* conformation was preferred when the concentration of acetamide molecules was low (i.e., electrolyte with molar ratio of 1:2) because it can help to reduce the repulsion between Li cations in close contact in the electrolyte.
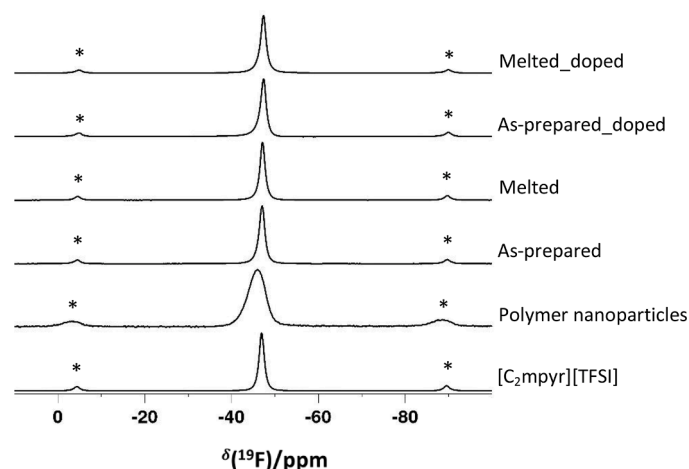

Fig. 9. Fitting static ^{19}F NMR CSA patterns of [C₂mpyr][TFSI] at 20°C for three different conformations of the TFSI anion.

However, a higher fraction of TFSI anions adopted the *cis* conformation in the electrolyte with high acetamide concentration where strong interactions between the TFSI anions and Li cations with acetamide occur. Finally, the authors observed that TFSI anions adopted preferentially the *trans* conformation with lower energy in the electrolyte with molar ratio of 1:4. The *cis* and *trans* conformations have also been observed by solid-state NMR, showing different isotropic chemical shifts [31].

The single isotropic signal we have observed in the MAS spectrum indicates that these three conformations must undergo exchange on the timescale of the MAS NMR signal acquisition (around 5 ms). The assignment of these distinct CSA patterns to specific conformations would require the parameters to be calculated from the different structures, which is beyond the scope of this article. Further evidence for the exchange between these sites is provided by the evolution of the spectral line shapes as the temperature and echo time are varied (Fig. S4).

3.5. Solid-state NMR analysis: dynamics

The analysis of SSNMR line widths and T_1 relaxation times were employed in this study. These experiments are sensitive to rotational and translational dynamics, and quantitative and qualitative information on dynamics can be extracted from these parameters based on their temperature dependence. The ion dynamics in the OIPC, polymer nanoparticles and composites were studied using solid-state ^{19}F, ^{1}H and ^{7}Li NMR carried out on static samples.

3.5.1. Line width analysis

Polymer nanoparticles. The effect of temperature on the lithium environment and dynamics in the pure polymer nanoparticles was studied by ^{7}Li single pulse static NMR experiments with the sample heated from 20 to 160 °C, followed by cooling (Fig. 10). During heating from 20 to 100 °C, the [7]Li line width decreases from around 2000 to 1200 Hz, reflecting increased dynamics of the Li cations such as faster ion jumps that result in motional averaging [17,32]. A dramatic increase in the [7]Li line widths is then seen above 100 °C, reaching around 3400 Hz at 160 °C. When the sample is cooled from 160 °C a further increase of the line width values is observed.

This behaviour is related to the reorganization of the polymer structure. Initially, the lithium ions are located primarily on the surface of polymer nanoparticles associated with the anion of the side chain, and

Fig. 8. ^{19}F MAS NMR spectra of [C₂mpyr][TFSI], polymer, 25:75 v% polymer nanoparticles:[C₂mpyr][TFSI] composites as prepared (as-prepared) and after melting the OIPC component (melted), and Li doped composites as prepared (as-prepared_doped) and after melting the OIPC component (melted_doped). Side bands are indicated with (*) in each spectrum.
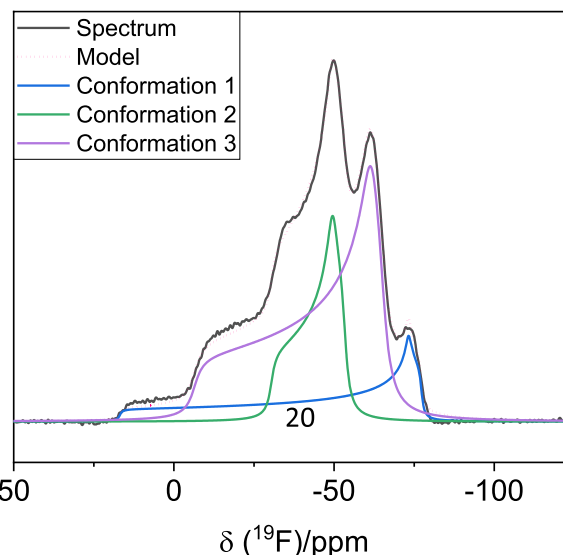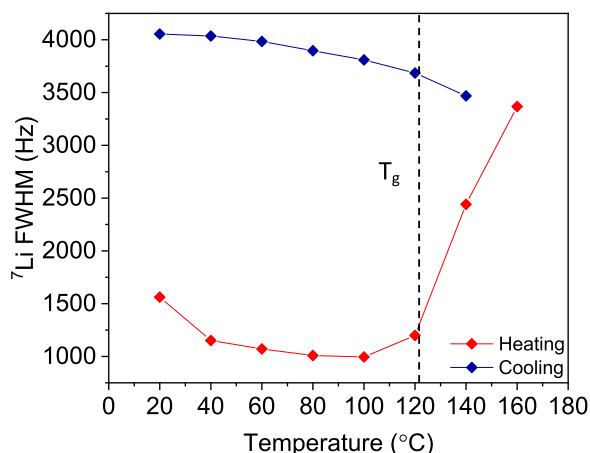
Fig. 10. ^{7}Li line widths of polymer nanoparticles obtained at a range of temperatures between 20 and 160 °C, the vertical dashed line indicates the glass transition temperature of the polymer at 122 °C.

they are surrounded by free volume. Above the glass transition temperature of the polymer (122 °C) the polymer chains become dynamic and entangle, resulting in the agglomeration of the polymer particles. This process is irreversible, so when the temperature decreases the nanoparticles remain agglomerated and a large fraction of the lithium cations originally located at the particle surfaces are instead trapped within the bulk agglomerated polymer, thereby restricting their mobility. This results in the increased ^{7}Li NMR line widths above 100 °C. These line widths further broaden upon cooling due to a further reduction in lithium mobility which reduces motional averaging. This will be very detrimental to the composite electrolyte performance, which is why the maximum temperature used in the other studies of this work was restricted to below the polymer T_g.

Polymer nanoparticles: [C$_2$mpyr][TFSI] composites and Li salt effect. The ion dynamics in the pure OIPC, polymer nanoparticles and the as-prepared composites and composites after melting the OIPC component, were analysed via variable temperature ^{7}Li, ^{19}F and ^{1}H static NMR (selected spectra are shown in Figs. 11–13) in the temperature range from 20 to 80 °C. The linewidths and area fractions were determined by spectral deconvolution (see Fig. S4).

To compare the lithium mobility in the materials, the ^{7}Li static NMR line widths during heating of the polymer nanoparticles and the composites are presented in Fig. 11. ^{7}Li has a spin 3/2 and can therefore exhibit multi component T_2 relaxation leading to the appearance of two distinct line width components when the quadrupolar interactions governs the relaxation [33]. However, this effect is not usually observed in these types of composite materials, i.e., organic ionic plastic crystals and polymers or OIPCs doped with Li salt. Rather, ^{7}Li solid-state NMR spectra (as well as those of other nuclei as ^{1}H and ^{19}F) of OIPC-based materials will typically show two populations corresponding to mobile/diffusive ions and less mobile or static ions, whose relative fractions will change with temperature [20].

The composite as-prepared ^{7}Li line widths are significantly broader than for the pure polymer as a result of the restriction of motion at the polymer surface due to the surrounding OIPC. Measured line widths after melting the OIPC in the composite (i.e., melted) are smaller compared with as-prepared composite up to 50 °C. At higher temperatures, both composites describe a similar trend with a slight increase of the line widths in melted with respect to as-prepared. This observation agrees with the formation of the composite interphase with increased structural disorder discussed above (see thermal analysis, Section 3.1.1), in which the lithium ions are more mobile and support the increase in ion conductivity observed in melted with respect to as-prepared.

Line widths determined from ^{7}Li static NMR spectra for composites

as-prepared, melted, as-prepared_doped and melted_doped show an increase in lithium-ion mobility with temperature in the composites as can be observed in Fig. 11a b c and d. Contrasting behaviour was observed in the doped composite along the phase transitions. The as-prepared_doped showed similar linewidths at low temperatures (i.e., in phase II) to melted, while the linewidths observed in the melted_doped were much narrower in this region and similar to the polymer linewidths. Interestingly, the ^{7}Li line widths appear to increase with increasing temperature in melted_doped, consistent with the cold crystallisation observed in phase I in the DSC results (Fig. 2c), which promotes a more ordered environment surrounding the Li ions that limits their mobility. The narrower ^{7}Li line width of composites as-prepared_doped and melted_doped with respect to the other materials demonstrates a more significant Li ion mobility once the polymer nanoparticles: OIPC composite is doped with the Li salt and it is consistent with previous studies of the Li-doped OIPC [20,34]. It may also be attributed to a further doping of the OIPC as a result of the exchange between the Li cations at the polymer nanoparticles surface with the OIPC cations. A further reduction after melting the OIPC in melted_doped is also observed and can be attributed to a further mixing of the Li salt with other composite components after melting the OIPC.

As discussed above, the ^{19}F static NMR spectrum of the pure [C$_2$mpyr][TFSI] OIPC shows a departure from a typical single ^{19}F CSA pattern, suggesting the presence of multiple fluorine environments likely corresponding to the *cis, trans* and *gauche* conformations and undergoing exchange as discussed above. The ^{19}F line shape for the pure polymer nanoparticles shows a very similar shape reflecting the same TFSI-based chemical structure but appearing more broadened due to increased local disorder (and potentially also dynamics) in the polymer compared with the crystalline OIPC. The ^{19}F spectra remain broad in the pure OIPC and the polymer nanoparticles when the temperature is increased from 20 to 50 °C, indicates that the TFSI groups are not undergoing isotropic rotational dynamics on the *µ*s timescale (Fig. 12a).

A combination of narrow and broad ^{19}F NMR line shape components are present in as-prepared composite from 20 °C to 70 °C and in as-prepared_doped composite from 40 °C to 70 °C during the first heating, note that at 20 °C a CSA pattern is observed, and a narrow component could not be extracted (Fig. 12b and d). This effect is commonly observed in both pure OIPC and OIPC composites. The narrow peaks are caused by motional averaging of the ^{19}F CSA and correspond to a fraction of anions undergoing isotropic rotation, while the broad component reflects the less mobile ions [15]. The fraction of the narrow peak increases with temperature for both composites and higher fractions are observed in the undoped composite at lower temperatures while slightly smaller fractions are observed in the Li doped composite.

A further increase in the fraction of the mobile component can be observed during a second heating (after melting the OIPC component at 90 °C) in the polymer nanoparticles: OIPC composite (melted). While the highest fractions of mobile anions are observed in the composite doped with Li salt after melting the OIPC component, melted_doped, the TFSI ions mobility at first seems to become more hindered with increasing temperature. Again, this is likely due to the cold crystallisation observed during the thermal analysis, where, similarly to the discussion regarding the Li ions mobility, a more ordered structural environment around the TFSI ions limits their mobility (see Fig. 12c and d).

The addition of the polymer nanoparticles to the OIPC creates disorder in the lattice, disrupts the ordered crystalline structure of the OIPC and allows the fraction of the TFSI anions present in the interfacial regions to become mobile (no mobile anion fraction was observed in the pure OIPC over this temperature range). However, the degree of disorder in the interfacial regions varies between the composites. The as prepared composites as-prepared and as-prepared_doped are characterised by more ordered interfacial regions that leads to lower ^{19}F area fractions indicating that TFSI ions mobility is limited in these materials. On the other hand, after melting the OIPC component in the composites, the contact between the OIPC and the polymer in the case of the melted
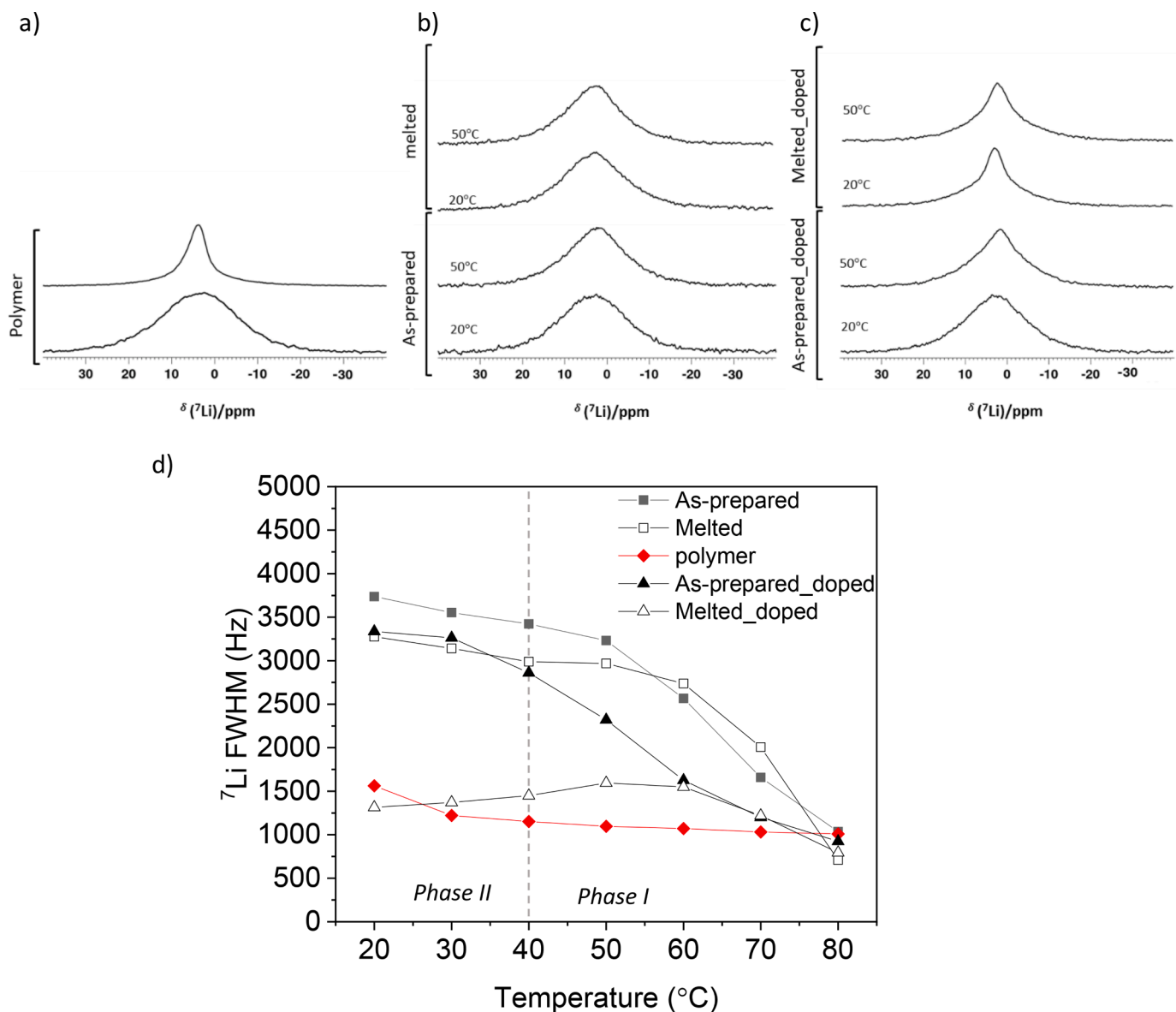
Fig. 11. Static ^{7}Li Hahn echo NMR spectra at 20 ˚C and 50 ˚C of (a) polymer nanoparticles, (b) 25:75 v% polymer nanoparticles: OIPC composites as prepared (as-prepared) and after melting the OIPC component (melted), (c) Li doped composites as prepared (as-prepared_doped) and after melting the OIPC component (melted_doped) and d) ^{7}Li NMR line widths as a function of the temperature of the composites as-prepared, melted, as-prepared_doped and melted_doped.

composite increases and facilitates the mobility of TFSI groups in the interphase. Further structural disorder is created in the interphase after doping the composite, i.e., in melted_doped composite, which leads to a higher fraction of mobile TFSI ions.

The broad ^{1}H NMR peak observed in the pure OIPC indicates that the [C$_2$mpyr] cations show strong homonuclear dipolar interactions (Fig. 13a). In the polymer a much broader ^{1}H peak is observed at 20 ˚C, reflecting the much more disordered structure (and also less dynamics) compared to the OIPC, but at 50 ˚C this peak is seen to narrow significantly, indicating that a fraction of the protons in the polymer groups increase their mobility with temperature even below the glass transition.

The ^{1}H NMR spectra of the polymer nanoparticles: OIPC composite as-prepared show a broad peak at 20 °C that gets slightly narrower with temperature (Fig. 13b and c) and reflects the motional averaging of the [C$_2$mpyr] cations. As with the ^{19}F, these spectra reflect overlapping signals from both the OIPC and the polymer itself. The increase in mobility cannot be attributed only to the interphase because as mentioned above at this temperature some protons also become mobile in the polymer. During the second heating a narrower peak is observed

in melted than as-prepared at 20 °C and remains unchanged at 50 °C. It indicates that the proton mobility in melted is enhanced by the interphase formation and remains with temperature.

Once the polymer nanoparticles: OIPC composite is doped with the LiTFSI salt, the ^{1}H NMR spectra show a similar trend to the ^{19}F spectra, with both a broad and narrow component observed during the first and second heating. The narrow peak fraction increases with temperature (Fig. 13c and d) with a further increase of the fraction of the mobile component in the melted_doped, composite, i.e., after melting the OIPC component. The area fraction decreases in this composite as it approaches phase I, once again following the trends observed in the ^{7}Li and ^{19}F linewidth analysis and consistent with the cold crystallisation phenomenon previously described. These observations show that the addition of Li salt into these composites, i.e., as-prepared_doped and melted_doped, promote even more the mobility of the OIPC cations compared with the polymer nanoparticles: OIPC composites. The incorporation of the Li salt increases the disorder and dynamics of the OIPC phase.

In general, these NMR data show that the interphase formed in the
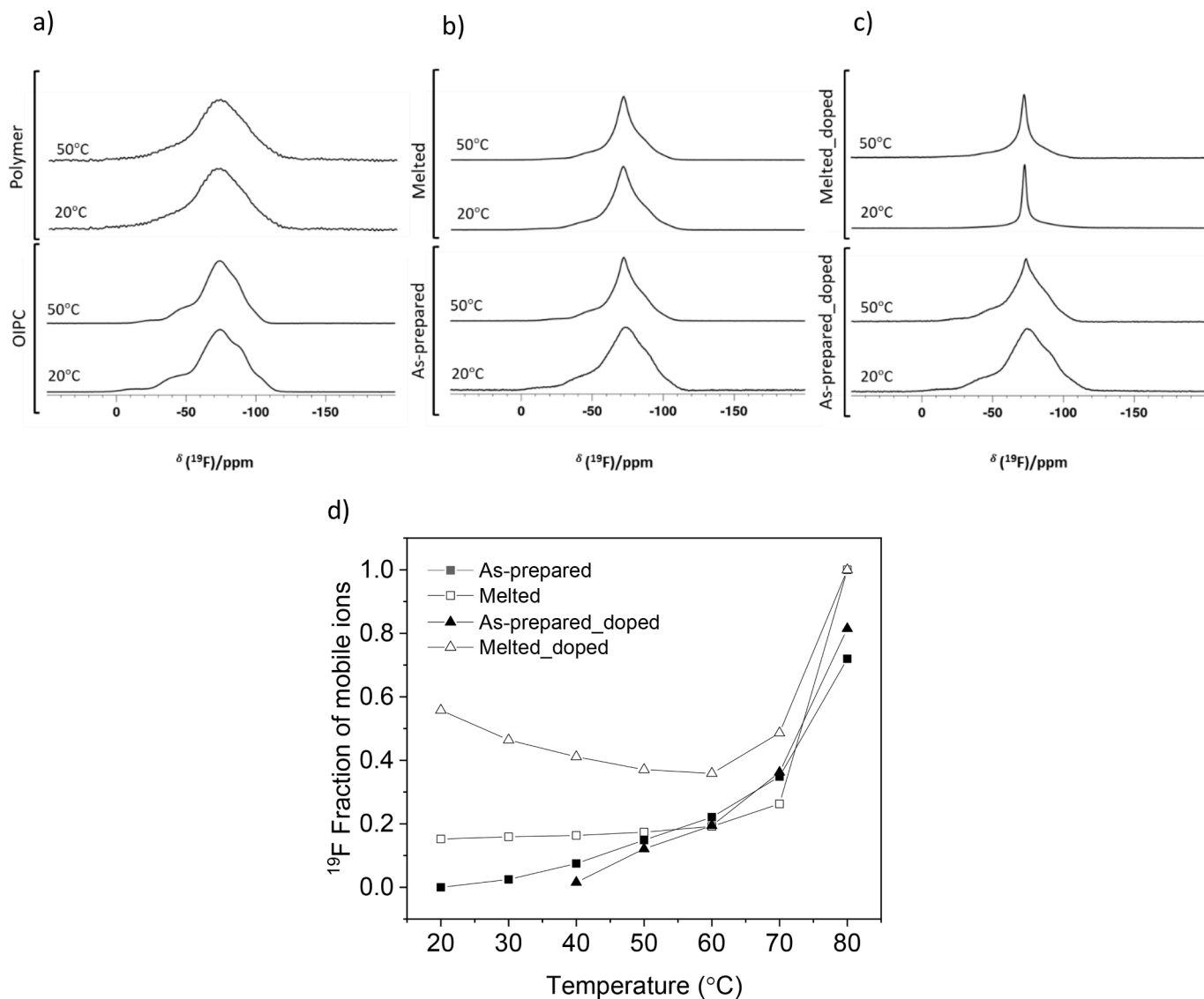
Fig. 12. Static ^{19}F Hahn echo NMR spectra at 20 and 50 °C of (a) OIPC and polymer nanoparticles, (b) 25:75 v% polymer nanoparticles: OIPC composites as prepared (as-prepared) and after melting the OIPC composite (melted), (c) Li doped composites as prepared (as-preprared_doped) and after melting the OIPC component (melted_doped) and (d) ^{19}F area fraction of the narrow component as a function of the temperature of the composites as-prepared, melted, as-prepared_doped and melted_doped.

polymer nanoparticles: OIPC composites promotes the mobility of lithium ions, as well as a fraction of the OIPC anions and cations thereby explaining the observed increase in ion conductivity, which will be contributed to by the average mobility of all of these charged species in the composites as-prepared, melted and melted_doped. The increase in ion mobility observed in the as-prepared_doped composite also explains the similar ion conductivity of this material to the pure OIPC. Additionally, the broad and narrow peaks observed during the line shape analysis are consistent with the presence of submicrometric crystals and significant fractions of disordered grain boundaries as observed in the morphology studies.

3.5.2. T_1 relaxation times

Information about ion dynamics was also extracted via measurement of the spin-lattice (T_1) relaxation times of ^{19}F and ^{7}Li of [C$_2$mpyr][TFSI], the polymer nanoparticles, and composites (i.e., as-prepared, melted, as-prepared_doped and melted_doped These times were measured during heating of the samples from 20 °C to 80 °C (see Fig. 14a and b).

The T_1 relaxation time is a measure of the timescale of the return of the nuclear magnetisation to thermal equilibrium, a process driven by

dynamics occurring on frequencies at or near the resonance (Larmor) frequency. These dynamics, such as molecular rotations, are thermally driven processes with an associated activation energy E_A. A T_1 minimum is observed when the inverse of the motional correlation time matches the Larmor frequency and therefore causes the most efficient longitudinal relaxation. The dependency of T_1 with temperature, in the simplest cases where a single relaxation mechanism is present, is then described by a characteristic V-shape. Therefore, depending on the frequency of the dynamics driving the relaxation, T_1 values can either increase or decrease with temperature (as seen in Fig. 14). ^{1}H T_1 values are not presented due to the overlapping signals from the OIPC and polymer hindering the analysis of the data.

The ^{7}Li T_1 relaxation times of the polymer nanoparticles and composites measured as a function of temperature are shown in Fig. 14a. ^{7}Li T_1 values are sensitive to jumps of the Li ions between different sites, as well as the rearrangement of the local structure around the Li. A general trend of decreasing T_1 values with increasing temperature is observed where the composites show a greater variation with temperature compared with the polymer. A sudden decrease in the T_1 value of as-prepared is observed at 40 °C when the OIPC transitions from phase II
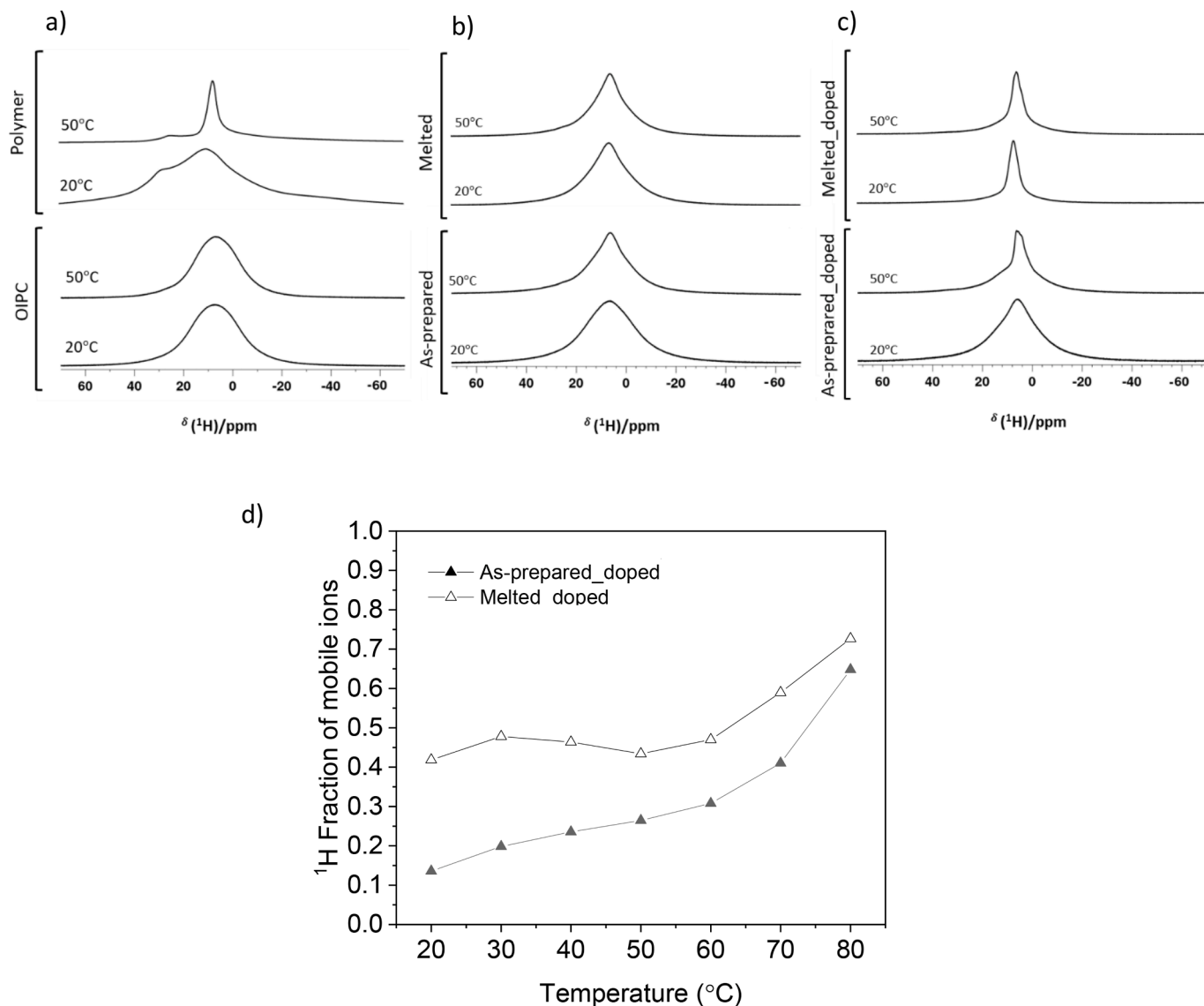
Fig. 13. Static ^{1}H NMR spectra at 20 and 50 °C of (a) OIPC and polymer nanoparticles, (b) 25:75 v% polymer nanoparticles: [C$_2$mpyr][TFSI] composites as prepared (as-preprared) and after melting the OIPC component (melted), (c) Li doped composites as prepared (as-prepared_doped) and after melting the OIPC (melted_doped) and (d) ^{1}H area fraction of the narrow component as a function of the temperature of the composites as-prepared_doped and melted_doped.
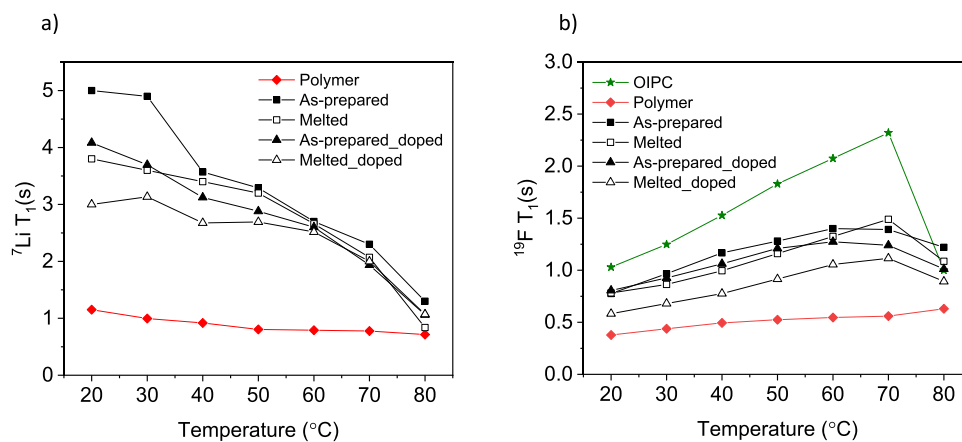

Fig. 14. Plots of the overall (a) ^{7}Li and (b) ^{19}F and T$_1$ relaxation times as a function of temperature for the OIPC, the polymer nanoparticles, 25:75 v% polymer nanoparticles: OIPC composite as prepared (as-prepared) and after melting the OIPC component (melted) and Li doped composites as prepared (as-prepared_doped) and after melting the OIPC component (melted_doped).

to I (see thermal analysis, Section 3.1.1.), this behaviour is not observed in melted composite which showed T_1 values lower than as-prepared even after melting the OIPC component at 80 °C and indicating higher Li dynamics in the phase II of melted. This observation can be attributed to more local structural disorder in the OIPC in melted compared with as-prepared because of the interphase formation (see Sections 3.1 and 3.2).

A reduction in the ^{7}Li T_1 values with temperature is also observed after doping the composite with Li salt. However, the T_1 values of as-prepared_doped were shorter than melted at 20 °C and 40 °C and longer at higher temperatures. These observations indicate that the Li dynamics along phase I is lower in as-prepared_doped than in melted but higher in phase II. This also agrees with our ^{7}Li linewidth observations where Li mobility is also restricted in phase I and facilitated in phase II. After melting the OIPC component further shortened T_1 values can be seen in both phase II and I indicating increased Li ion mobility. As the samples approach their melting temperatures and transition to the liquid state allowing a higher Li mobility (see Section 3.1), the relaxation times become similar for all of them.

^{7}Li T_1 values are lowest of all in the pure polymer nanoparticles. This suggests different dynamics in the composites and the polymer, and this can be understood in a similar way to the ^{7}Li line width measurements discussed above. For the pure polymer, the Li ions located at the nanoparticle surfaces are surrounded by free volume and thus have a large degree of freedom to move. In the case of the as prepared composite, the Li ions located at the surface of the polymer nanoparticles become surrounded by the OIPC, and this can restrict their mobility. On the other hand, the restricted Li ion mobility in the melted composite is countered by the interphase formed between the OIPC and the polymer that forms and promotes local disorder, so the ions can move more freely again. As the temperature increases, the dynamics of the melted composite tend to be like the polymer, where the Li ions associated with the anionic side chains seem to be more dynamic due to the surrounding free volume. Further disorder in the interphase is created once the polymer-based composite is doped with Li salt and this further increases the local mobility of the Li ions with the temperature with the exception of the as-prepared_doped composite along phase I where the Li mobility is restricted indicating a more organised interfacial region than the interphase in melted composite.

The ^{19}F T_1 relaxation times as a function of temperature are presented in Fig. 14b. These values will be sensitive to both the rotations of the CF_3 groups, as well as reorientations of the TFSI anions as a whole. When the temperature of the OIPC is increased from 20 to 70 °C, the ^{19}F T_1 values increase. As with the decreasing ^{7}Li T_1 values, this reflects increasing dynamics of the anionic groups in the material, in this case in the temperature regime above the T_1 minimum. Once the OIPC reaches the melting temperature, the liquid state allows a high mobility of the anion, and this results in the onset of additional dynamic modes and a resulting decrease in the ^{19}F T_1 at 80 °C.

In the case of the OIPC, all the anions are surrounded by closely packed cations and may undergo isotropic rotation, while for the pure polymer beads the anions are on the end of the polymer nanoparticle side chains which "dangle" into free space and will restrict full reorientation. It is important to note that the ^{19}F NMR signals measured from the polymer-based composites reflect a predominant contribution of TFSI anions in the OIPC and a minor contribution of TFSI groups on the polymer (Fig. 14b).

The melted composite showed similar ^{19}F T_1s to as-prepared, implying similar TFSI dynamics at this timescale. After doping the polymer-based composite the longer T_1 values shown in as-prepared_doped than melted_doped indicate that the anion dynamics are restricted as a result of a more organized chemical environment in an OIPC-based interfacial region as was discussed in Section 3.1. On the other hand, in the other composite, i.e., melted_doped, the ions can interact with the Li salt and promote structural disorder in the interphase leading to more TFSI anion mobility.

4. Conclusions

The phase behaviour, structure and dynamics of solid electrolyte composites between lithium functionalised polymer nanoparticles and the organic ionic plastic crystal [C_2mpyr][TFSI] were investigated. The thermal properties, morphology, ion conductivity, and structural and dynamics studies of the composites as prepared and after melting the OIPC component suggested a disruption of the crystalline lattice of the OIPC after adding the polymer nanoparticles leading to formation of disordered interfacial regions in the composites. Generally, the formation of more local structural disorder correlates with increased ion conductivity and ion dynamics of lithium, as well as the OIPC cations and anions, in these composites. After melting the OIPC component, the more intimate mixing of the OIPC and polymer at the interphase results in a further increase in local disorder and ion mobility. In addition, the Li doping of a selected composite with LiTFSI was studied. The interfacial regions formed were characterised by additional disorder compared with the polymer-based composites leading to further increases in dynamics of lithium ions, and OIPC anions and cations.

These findings highlight the importance of understanding the properties of new interfacial regions of polymer electrolyte composites and the effect that interface regions can have on desired properties like Li ion dynamics and ionic conductivity. Further studies with different polymer morphologies and OIPCs chemistries are needed to design electrolytes with improved target properties.

Declaration of Competing Interest

The authors declare that they have no known competing financial interests or personal relationships that could have appeared to influence the work reported in this paper.

Data availability

Data will be made available on request.

Supplementary materials

Supplementary material associated with this article can be found, in the online version, at doi:10.1016/j.jmro.2023.100095.

References

[1] A. Marchetti, J. Chen, Z. Pang, S. Li, D. Ling, F. Deng, X. Kong, Understanding surface and interfacial chemistry in functional nanomaterials via solid-state NMR, Adv. Mater. 29 (2017).

[2] A. Salvadori, D. Grazioli, Computer Simulation For Battery Design and Lifetime Prediction, Elsevier Ltd., 2015.

[3] J.B. Goodenough, H.D. Abruna, M.V. Buchanan, Basic research needs for electrical energy storage report of the basic energy sciences workshop on electrical energy storage, 2007.

[4] S. Wei, S. Choudhury, Z. Tu, K. Zhang, L.A. Archer, Electrochemical interphases for high-energy storage using reactive metal anodes, Acc. Chem. Res. 51 (2018) 80–88.

[5] C.W. Monroe, C. Monroe, J. Newman, The effect of interfacial deformation on electrodeposition kinetics the effect of interfacial deformation on electrodeposition kinetics, (2015).

[6] A. Manthiram, X. Yu, S. Wang, Lithium battery chemistries enabled by solid-state electrolytes, Nat. Rev. Mater. 2 (2017) 1–16.

[7] Y. García, L.A. O'Dell, Understanding the interfacial region in organic ionic plastic crystal composite electrolyte materials by solid-state NMR, Curr. Opin. Colloid Interface Sci. 61 (2022), 101632.

[8] X. Wang, R. Kerr, F. Chen, N. Goujon, J.M. Pringle, D. Mecerreyes, P. C. Howlett, Toward high-energy-density lithium metal batteries: opportunities and challenges for solid organic electrolytes, Adv. Mater. 32 (2020) 1–21.

[9] M. Forsyth, J. Huang, D.R. MacFarlane, Lithium doped N-methyl-N-ethylpyrrolidinium bis(trifluoromethanesulfonyl)amide fast-ion conducting plastic crystals, J. Mater. Chem. 10 (2000) 2259–2265.

[10] D.R. MacFarlane, P. Meakin, J. Sun, N. Amini, M. Forsyth, Pyrrolidinium imides: a new family of molten salts and conductive plastic crystal phases, J. Phys. Chem. B 103 (1999) 4164–4170.

[11] F. Nti, L. Porcarelli, G.W. Greene, H. Zhu, F. Makhlooghiazad, D. Mecerreyes, P. C. Howlett, M. Forsyth, X. Wang, The influence of interfacial interactions on the conductivity and phase behaviour of organic ionic plastic crystal/polymer nanoparticle composite electrolytes, J. Mater. Chem. A 8 (2020) 5350–5362.

[12] P. Lu, S.J. Harris, Lithium transport within the solid electrolyte interphase, Electrochem. Commun. 13 (2011) 1035–1037.

[13] D. Aurbach, E. Pollak, R. Elazari, G. Salitra, C.S. Kelley, J. Affinito, On the surface chemiscal aspects of very high energy density, rechargeable Li-sulfur batteries, J. Electrochem. Soc. 156 (2009) A694–A702.

[14] S. Haber, M. Leskes, What can we learn from solid state NMR on the electrode–electrolyte interface? Adv. Mater. 30 (2018) 1706496–1706506.

[15] H. Zhu, L.A. O'Dell, Nuclear magnetic resonance characterisation of ionic liquids and organic ionic plastic crystals: common approaches and recent advances, Chem. Commun. 57 (2021) 5609–5625.

[16] F. Nti, G.W. Greene, H. Zhu, P.C. Howlett, M. Forsyth, X. Wang, Anion effects on the properties of OIPC/PVDF composites, Mater. Adv. 2 (2021) 1683–1694.

[17] Y.V. Oza, D.R. Macfarlane, M. Forsyth, L.A. O'Dell, Characterisation of ion transport in sulfonate based ionomer systems containing lithium and quaternary ammonium cations, Electrochim. Acta 175 (2015) 80–86.

[18] L. Meabe, T.V. Huynh, D. Mantione, L. Porcarelli, C. Li, L.A. O'Dell, H. Sardon, M. Armand, M. Forsyth, D. Mecerreyes, UV-cross-linked poly(ethylene oxide carbonate) as free standing solid polymer electrolyte for lithium batteries, Electrochim. Acta 302 (2019) 414–421.

[19] X. Wang, H. Zhu, G.W. Greene, Y. Zhou, M. Yoshizawa-Fujita, Y. Miyachi, M. Armand, M. Forsyth, J.M. Pringle, P.C. Howlett, Organic ionic plastic crystal-based composite electrolyte with surface enhanced ion transport and its use in all-solid-state lithium batteries, Adv. Mater. Technol. 2 (2017) 1–6.

[20] F. Nti, H. Ueda, C.S.M. Kang, G.W. Greene, J.M. Pringle, H. Zhu, P. Howlett, M. Forsyth, X. Wang, Ion transport in Li-doped triethyl(methyl)phosphonium tetrafluoroborate (Li-[P 1222][BF 4]) impregnated with PVDF nanoparticles, J. Phys. Chem. C 126 (2022) 3839–3852.

[21] L. Porcarelli, P. Sutton, V. Bocharova, R.H. Aguirresarobe, H. Zhu, N. Goujon, J. R. Leiza, A. Sokolov, M. Forsyth, D. Mecerreyes, Single-ion conducting polymer nanoparticles as functional fillers for solid electrolytes in lithium metal batteries, ACS Appl. Mater. Interfaces 13 (2021) 54354–54362.

[22] F. Makhlooghiazad, L.A. O'Dell, L. Porcarelli, C. Forsyth, N. Quazi, M. Asadi, O. Hutt, D. Mecerreyes, M. Forsyth, J.M. Pringle, Zwitterionic materials with disorder and plasticity and their application as non-volatile solid or liquid electrolytes, Nat. Mater. 21 (2022) 228–236.

[23] A. Bielecki, D.P. Burum, Temperature dependence of 207Pb MAS spectra of solid lead nitrate an accurate, sensitive thermometer for variable-temperature MAS, J. Magn. Reson. Ser. A 116 (1995) 215–220.

[24] D.R. MacFarlane, P. Meakin, N. Amini, M. Forsyth, Structural studies of ambient temperature plastic crystal ion conductors, J. Phys. Condens. Matter 13 (2001) 8257–8267.

[25] J. Huang, M. Forsyth, D.R. MacFarlane, Solid state lithium ion conduction in pyrrolidinium imide-lithium imide salt mixtures, Solid State Ionics 136–137 (2000) 447–452.

[26] J.M. Pringle, Recent progress in the development and use of organic ionic plastic crystal electrolytes, Phys. Chem. Chem. Phys. 15 (2013) 1339–1351.

[27] A. Tagaya, Encyclopedia of Polymeric Nanomaterials, Springer-Verlag, Berlin Heidelberg, 2013, pp. 1–6, in: Encycl. Polym. Nanomater.

[28] F. Ramos-Saz, Y. García, C.S.M. Kang, L.A. O'Dell, M. Forsyth, J.M. Pringle, Exploring the influence of the cation type and polymer support in bis (fluorosulfonyl)imide-based plastic crystal composite membranes for CO 2 /N 2 separation, J. Mater. Chem. A (2021).

[29] L. Jin, K.M. Nairn, C.D. Ling, H. Zhu, L.A. O'Dell, J. Li, F. Chen, A.F. Pavan, L. A. Madsen, P.C. Howlett, D.R. Macfarlane, M. Forsyth, J.M. Pringle, Conformational dynamics in an organic ionic plastic crystal, J. Phys. Chem. B 121 (2017) 5439–5446.

[30] S. Li, Z. Cao, Y. Peng, L. Liu, V. Wang, S. Wang, J.Q. Wang, T. Yan, X.P. Gao, D. Y. Song, P.W. Shen, Molecular dynamics simulation of LiTFSI-acetamide electrolytes: structural properties, J. Phys. Chem. B 112 (2008) 6398–6410.

[31] Y. Chen, N.R. Jaegers, K.S. Han, H. Wang, R.P. Young, G. Agarwal, A.S. Lipton, R. S. Assary, N.M. Washton, J.Z. Hu, K.T. Mueller, V. Murugesan, Probing conformational evolution and associated dynamics of Mg(N(SO2CF3)2) 2·dimethoxyethane adduct using solid-state 19F and 1H NMR, J. Phys. Chem. C 124 (2020) 4999–5008.

[32] P.C.M.M. Magusin, I.D. Seymour, O. Pecher, C.P. Grey, NMR studies of electrochemical storage materials, in: Mod. Methods Solid-State NMR A Pract. Guid., 2018: pp. 322–327.

[33] M.I. Gordon, M.J.R. Hoch, Quadrupolar spin-lattice relaxation in solids, J. Phys. C Solid State Phys. 11 (1978) 783–795.

[34] N. Iranipour, D.J. Gunzelmann, A.J. Seeber, J. Vongsvivut, A.F. Hollenkamp, M. Forsyth, P.C. Howlett, Effect of secondary phase on thermal behaviour and solid-state ion conduction in lithium doped N-ethyl-N-methylpyrrolidinium tetrafluoroborate organic ionic plastic crystal, J. Mater. Chem. A 5 (2017) 24909–24919.